Key Points:
- We present the first calculations of FeO partitioning between ferropericlase and liquid iron at Earth's core conditions
- Partitioning is larger than previous extrapolated estimates and depends strongly on oxygen content
- O flux through solid mantle is limited and unlikely to explain outer core stable stratification; flux from a molten mantle is much greater

Correspondence to:
C. J. Davies,
c.davies@leeds.ac.uk

Partitioning of Oxygen Between Ferropericlase and Earth's Liquid Core

C. J. Davies[1] [ID]**, M. Pozzo[2]** [ID]**, D. Gubbins[1], and D. Alfè[2,3]** [ID]

[1]School of Earth and Environment, University of Leeds, Leeds, UK, [2]Department of Earth Sciences and Thomas Young Centre @ UCL, UCL, London, UK, [3]London Centre for Nanotechnology, UCL, London, UK

Abstract Transfer of oxygen between Earth's core and lowermost mantle is important for determining the chemistry and nature of stratification on both sides of the core-mantle boundary (CMB). Previous studies have found that oxygen enters the metal when Fe-O liquid equilibrates with representative lower mantle materials. However, experiments have not yet been conducted at CMB pressure-temperature conditions. Here we use density functional theory to obtain the first estimates of oxygen partitioning between liquid Fe-O-Si metals and ferropericlase at CMB conditions. Our method successfully reproduces experimentally derived partitioning data at 134 GPa and 3200 K, while our calculations show a strong increase of oxygen partitioning into metal with temperature and a weaker increase with pressure, consistent with previous work. At CMB conditions of 135 GPa and 4000–4700 K oxygen partitioning into metal is higher than previous estimates and increases strongly with metal oxygen concentration. Analysis of the lower mantle chemical boundary layer shows that oxygen transport through the solid is severely limited even with the enhanced partitioning and is unlikely to explain the thickness of a stably stratified layer below the CMB inferred from seismology. However, if the lower mantle was molten in early times, as suggested by core evolution models with high thermal conductivity, then the mass flux and stable layer thickness are significantly increased.

Plain Language Summary Earth's core is composed primarily of iron, silicon, and oxygen; it is directly below the solid mantle, which is mainly composed of two different minerals called bridgmanite and ferropericlase. Here we present the first calculations of iron oxide partitioning between ferropericlase and liquid iron-silicon-oxygen mixtures at core-mantle boundary (CMB) pressure-temperature-concentration conditions. Partitioning of iron oxide between the core and mantle is important for constraining the chemistry on either side of the CMB, determining the composition of the core, and elucidating the origin of the seismically detected stable layer at the top of the core (which has previously been ascribed to FeO transfer from the mantle). We find that FeO partitioning into the core is stronger than found by previous studies at lower pressures and temperatures and is particularly sensitive to oxygen content in the metal. We analyze transfer of O through the lower mantle chemical boundary layer by diffusion and dynamic instability and find that in both cases, oxygen flux is smaller than previous estimates even with the greater partitioning. The resulting thickness of the chemically stable layer that arises below the CMB is too small to explain the seismic observations.

1. Introduction

At present, Earth's lower mantle is thought to comprise approximately 70–80% $(Mg,Fe)SiO_3$ bridgmanite, 15–20% $(Mg,Fe)O$ ferropericlase, and a small amount of calcium perovskite (Garnero et al., 2016). The liquid core is 5–10% lighter than pure iron, the main light elements based on cosmochemical abundances and core formation models being sulfur, silicon, and oxygen (Hirose et al., 2013; Nimmo, 2015; Rubie, Nimmo, et al., 2015). Recent studies of metal-silicate partitioning at the base of an ancient magma ocean have found that up to 7 wt% O and 8–9 wt% Si could have entered the core during its formation depending on the redox conditions of early Earth (Badro et al., 2015; Rubie, Jacobson, et al., 2015).

Oxygen is thought to be a crucial component of the core mixture since it is the only candidate element that has been shown to partition strongly into liquid iron on freezing at core conditions, which explains why the seismically observed inner core boundary (ICB) density jump of 0.8 ± 0.2 gm/cc (Masters & Gubbins, 2003)

is greater than expected from a pure solid-liquid phase transition (Alfè et al., 2002). Matching the seismic velocity and core mass requires another element and this can be achieved with S or Si, which partition almost evenly between solid and liquid iron (Alfè et al., 2002; Badro et al., 2014). Velocities and densities are calculated at ICB conditions from first principles for a variety of candidate core compositions and compared to the seismic and geodetic observations. Using this method, the molar concentrations of O and Si in the core, denoted $\bar{c}_O^c$ and $\bar{c}_{Si}^c$ respectively, are estimated as $\bar{c}_O^c = 0.08$–0.17 and $\bar{c}_{Si}^c = 0.02$–0.10 (Alfè et al., 2002; Badro et al., 2015; Davies et al., 2015).

Partitioning of O, S, and Si depresses the melting point at the ICB by up to 1000 K (Davies et al., 2015), while O partitioning during inner core growth drives compositional convection that helps power the dynamo process generating Earth's magnetic field. It is generally believed that most of the core's light element inventory was determined by metal-silicate separation and chemical equilibration at pressure-temperature-composition conditions of an early magma ocean (Rubie, Nimmo, et al., 2015), but the amount of O sequestered into the core during its formation is uncertain (Badro et al., 2015; Rubie, Jacobson, et al., 2015). Oxygen transfer (as FeO) after core formation could produce stable stratification below the core-mantle boundary (CMB; Buffett & Seagle, 2010) that persists to the present day (Helffrich & Kaneshima, 2010). The extent of post core formation O transfer depends crucially on its partitioning behavior at CMB conditions.

Previous studies suggest that FeO will enter the metal when representative lower mantle assemblages are placed in contact with liquid iron (Asahara et al., 2007; Frost et al., 2010; Knittle & Jeanloz, 1991; Ozawa et al., 2008; Takafuji et al., 2005). These experiments are extremely challenging, and the vast majority are necessarily conducted at upper/middle-mantle pressure-temperature conditions (Asahara et al., 2007; Frost et al., 2010; Knittle & Jeanloz, 1991; Takafuji et al., 2005), with very few measurements at lowermost mantle pressures (Ozawa et al., 2008). Frost et al. (2010) determined partitioning through a thermodynamic model that was compared to experimental data in the accessible range. However, the role of temperature and composition at CMB pressures has not been directly measured or calculated and is presently unknown. Increasing metal oxygen content is found to increase oxygen partitioning into the metal at experimentally accessible conditions (Tsuno et al., 2013); however, this positive feedback tends to yield unstable parameterizations when extrapolating the data (Fischer et al., 2015). A wide range of FeO partitioning results have therefore been obtained from extrapolations of experimentally determined data to CMB conditions: estimates of the oxygen distribution coefficient $K_D(O) = \bar{c}_{Fe}^c \times \bar{c}_O^c / \bar{c}_{Fe}^m$ range between $K_D(O) \sim 0.7$ (Ozawa et al., 2008) and $K_D(O) \sim 4$ (Frost et al., 2010). Here $\bar{c}_{Fe}^c$ is the molar Fe concentration in the metal (superscript c denotes the core, and overbars denote molar concentrations), and $\bar{c}_{Fe}^m$ is the molar concentration of Fe in ferropericlase (superscript m denotes the mantle).

Here we obtain the chemical potentials of iron in $Mg_{1-x}Fe_xO$, and oxygen in an $Fe_{1-x-y}Si_xO_y$ liquid at CMB conditions. Crucially, we are able to calculate directly the dependence of partitioning on composition at these conditions. Methods are described in section 2, and results, including a direct comparison with experimental data at 134 GPa and 3200 K, are presented in section 3. Discussion and an analysis of the chemical boundary layer above the CMB are given in section 4.

2. Methods

The techniques employed in this study have been used to calculate chemical potentials and partitioning of oxygen, sulfur, and silicon in solid and liquid iron at ICB conditions (Alfè et al., 2002). Oxygen equilibrium at the CMB between solid $Mg_{1-x}Fe_xO$ and liquid $Fe_{1-x-y}Si_xO_y$ is determined by the chemical potential of FeO in the core (μ_{FeO}^{core}) and mantle (μ_{FeO}^{mantle}) with thermodynamic equilibrium obtained for

$$\mu_{FeO}^{mantle} = \mu_{FeO}^{core} = \mu_{Fe}^{core} + \mu_O^{core}. \tag{1}$$

It is useful to write

$$\mu_{FeO}^{mantle}(p, T, \bar{c}_{Fe}^m) = k_B T \ln \bar{c}_{Fe}^m + \tilde{\mu}_{FeO}^{mantle}(p, T, \bar{c}_{Fe}^m), \tag{2}$$

and similarly

$$\mu_{FeO}^{core}(p, T, \bar{c}_O^c) = k_B T \ln \bar{c}_O^c + \tilde{\mu}_O^{core}(p, T, \bar{c}_O^c) + \mu_{Fe}^{core}(p, T, \bar{c}_O^c) = k_B T \ln \bar{c}_O^c + \tilde{\mu}_{FeO}^{core}(p, T, \bar{c}_O^c). \tag{3}$$

The quantities $\tilde{\mu}_{FeO}^{mantle}(p, T, \bar{c}_{Fe}^m)$ and $\tilde{\mu}_{FeO}^{core}(p, T, \bar{c}_O^c)$ have been computed using thermodynamic integration (Alfè et al., 2002), in which the chemical potential difference between a solute X (O in the core and Fe in the mantle) and a solvent A (Fe in the core and Mg in the mantle) is obtained by adiabatically (slowly) transmuting A into X and calculating the reversible work performed in the process. In classical statistical mechanics the masses of the atoms enter the chemical potential in a trivial way, and so in the molecular dynamics simulations we set the masses of all atoms equal to the mass of iron (55.847 amu). The time step was 1 fs, and the temperature was controlled using a Nosé thermostat. Here we are only concerned with small values of the core O concentration, $\bar{c}_O^c$. The mantle FeO concentration is determined by the concentration of Fe, $\bar{c}_{Fe}^m$.

The condition of chemical equilibrium defines the oxygen distribution coefficient

$$K_D(O) = \frac{\bar{c}_{Fe}^c \bar{c}_O^c}{\bar{c}_{Fe}^m} = \bar{c}_{Fe}^c \exp\left[\left(\tilde{\mu}_{FeO}^{mantle} - \tilde{\mu}_{FeO}^{core}\right)/k_B T\right]. \tag{4}$$

To calculate the chemical potential of O in the liquid $\tilde{\mu}_O^{core}(p, T, \bar{c}_O^c)$, we used simulation cells including $N = 157$ atoms. Calculations performed with $N = 67$ atoms showed differences in the chemical potential of less than ~ 50 meV, and so the results obtained with $N = 157$ should be converged to within a much smaller error. The plane-wave (PW) cutoff was 400 eV. Tests performed with PW cutoffs up to 1,000 eV showed convergence of energy differences to better than ~ 1 meV but also showed that pressures are underestimated by ~ 2.2 GPa. The calculated pressures were therefore corrected for this value. All simulations were performed with the Γ point only; tests performed with a $2 \times 2 \times 2$ grid showed that the chemical potential differences between oxygen and iron were converged to within 20 meV.

For the solid we note that transmuting MgO into FeO only involves transmuting Mg into Fe. The chemical potential of pure MgO, $\mu_{MgO}^0(p, T)$, is obtained from

$$\mu_{MgO}^0 = \mu_{MgO_{perf}} + \mu_{MgO_{harm}} + \mu_{MgO_{anh}}, \tag{5}$$

where $\mu_{MgO_{perf}}$ is the energy of the perfect MgO crystal, $\mu_{MgO_{harm}}$ the contribution to the free energy in the harmonic approximation, computed with the small displacement method (Alfè, 2009), and $\mu_{MgO_{anh}}$ the remainder, which can be computed using thermodynamic integration (Alfè et al., 2002). We found that the anharmonic contribution to the chemical potential of MgO is -20 ± 0.2 meV and that to the chemical potential of FeO is -80 ± 15 meV. We used $4 \times 4 \times 4$ supercells (64 f.u.) and checked convergence of the results using cells up to $8 \times 8 \times 8$. The quasi-harmonic component of the free energy was obtained using a $2 \times 2 \times 2$ grid of **k**-points to sample the Brillouin Zone, a PW cutoff of 500 eV, and displacements of 0.01 Å. With these prescriptions the quasi-harmonic free energies $\mu_{MgO_{harm}}^0$ and $\mu_{Mg_{63}FeO_{64harm}}$ were converged to better than 1 and 10 meV, respectively.

To investigate the dependence of $\tilde{\mu}_{FeO}^{mantle}(p, T, \bar{c}_{Fe}^m)$ on Fe concentration, we performed additional calculations in which we replaced a second Mg atom with Fe. We have done that using several atomic configurations, including replacing two Mg nearest neighbors or two Mg at larger distances from each other. In all cases we found differences of less than 0.1 eV per formula unit, showing little FeO-FeO interaction. With a good approximation we can therefore assume that $\tilde{\mu}_{FeO}^{mantle}(p, T, \bar{c}_{Fe}^m)$ is constant with respect to concentration for expected mantle concentrations.

3. Results

The majority of our simulations are performed at CMB conditions: 135 GPa and temperatures above 4000 K (Table 1). To validate our approach, we also performed a suite of calculations at 134 GPa and 3200 K. At these conditions and a starting composition consisting of a powdered mixture of pure metal and $Mg_{81}Fe_{19}O$, Ozawa et al. (2008) found that $K_D(O) = 0.78^{+0.22}_{-0.17}$. In the range $1.2 \leq \bar{c}_O^c \leq 14$ mol% we find $K_D(O)$ increases with $\bar{c}_O^c$ as expected (Table 1). At $\bar{c}_O^c = 1.2$ and 2.5 mol% we obtain $K_D(O) = 1.4^{+0.28}_{-0.23}$, in very close agreement with the experimental value. The agreement would be even better if we take into account the 10% uncertainty in the experimental temperature (Ozawa et al., 2008). Further refinement of the comparison is clearly limited since we are comparing two technically challenging and fundamentally different techniques that are subject to their own unique uncertainties. Experimental difficulties include identifying melting in the sample (Anzellini et al., 2013; Ozawa et al., 2008), the potential for oxidation of the sample at high pressure and temperature

Table 1
Chemical Potential of Oxygen at Core-Mantle Boundary Conditions

$\bar{c}_O^c$ (mol% O)	$\bar{c}_{Si}^c$ (mol% Si)	T (K)	$\tilde{\mu}_{FeO}^{core} - \tilde{\mu}_{FeO}^{mantle}$ (eV)	$K_D(O)$	P	$R_{FeO}^{core} - R_{FeO}^{mantle}$ (eV)
2.5	0	4112	-0.77 ± 0.05	$8.57^{+1.33}_{-1.16}$	$8.79^{+1.33}_{-1.16}$	1.75 ± 0.10
15.3	0	4112	-0.90 ± 0.06	$10.74^{+2.34}_{-2.00}$	$12.68^{+2.34}_{-2.00}$	1.45 ± 0.12
28.0	0	4112	-0.89 ± 0.06	$8.88^{+2.27}_{-1.92}$	$12.33^{+2.27}_{-1.92}$	1.21 ± 0.12
2.5	0	4300	-0.87 ± 0.05	$10.20^{+1.51}_{-1.32}$	$10.46^{+1.51}_{-1.32}$	2.03 ± 0.10
15.3	0	4300	-1.08 ± 0.06	$15.61^{+3.24}_{-2.76}$	$18.44^{+3.24}_{-2.76}$	1.35 ± 0.12
28.0	0	4300	-1.04 ± 0.06	$11.92^{+2.91}_{-2.48}$	$16.56^{+2.91}_{-2.48}$	1.06 ± 0.12
2.5	0	4700	-1.19 ± 0.05	$18.41^{+2.48}_{-2.19}$	$18.88^{+2.48}_{-2.19}$	1.87 ± 0.10
15.3	0	4700	-1.27 ± 0.06	$19.49^{+3.67}_{-3.17}$	$23.01^{+3.67}_{-3.17}$	1.76 ± 0.12
28.0	0	4700	-1.27 ± 0.06	$16.57^{+3.67}_{-3.17}$	$23.01^{+3.67}_{-3.17}$	1.02 ± 0.18
2.5	7.6	4112	-0.73 ± 0.06	$7.65^{+1.45}_{-1.22}$	$7.85^{+1.45}_{-1.22}$	2.09 ± 0.16
15.3	7.6	4112	-0.86 ± 0.06	$9.59^{+2.09}_{-1.76}$	$11.32^{+2.09}_{-1.76}$	1.54 ± 0.14
21.7	7.6	4112	-0.97 ± 0.06	$12.10^{+2.85}_{-2.41}$	$15.45^{+2.85}_{-2.41}$	1.12 ± 0.12
28.0	7.6	4112	-1.03 ± 0.08	$13.18^{+4.64}_{-3.70}$	$18.30^{+4.64}_{-3.70}$	0.79 ± 0.18
1.2	0	3200	-0.095 ± 0.05	$1.39^{+0.28}_{-0.23}$	$1.41^{+0.28}_{-0.23}$	—
2.5	0	3200	-0.097 ± 0.05	$1.38^{+0.28}_{-0.24}$	$1.42^{+0.28}_{-0.24}$	—
13.4	0	3200	-0.33 ± 0.10	$2.88^{+1.45}_{-1.01}$	$3.31^{+1.45}_{-1.01}$	—
14.0	0	3200	-0.30 ± 0.05	$2.58^{+0.59}_{-0.50}$	$3.00^{+0.59}_{-0.50}$	—

Note. Core O concentration $\bar{c}_O^c$, core Si concentration $\bar{c}_{Si}^c$, temperature T, excess chemical potential difference of FeO between the core and the mantle, $\tilde{\mu}_{FeO}^{core} - \tilde{\mu}_{FeO}^{mantle}$ (Methods), distribution coefficient $K_D(O) = \bar{c}_{Fe}^c \times \bar{c}_O^c / \bar{c}_{Fe}^m$, partition coefficient $P = \bar{c}_{FeO}^c / \bar{c}_{FeO}^m = \bar{c}_O^c / \bar{c}_{Fe}^m$, and heat of reaction $R_h = R_{FeO}^{core} - R_{FeO}^{mantle}$ as one FeO unit is transferred from the mantle to the core. In defining P we have used the fact that the core FeO concentration is determined by the amount of O since FeO dissociates into Fe and O in the liquid, while in the mantle the concentration of FeO is equal to the concentration of Fe. All calculations are conducted at a pressure of 135 GPa except the bottom section, which are calculated at 134 GPa.

(Frost et al., 2010), and diffusion of oxygen out of the liquid metal as the sample is quenched (Geßmann & Rubie, 1998; O'Neill et al., 1998). Our current theoretical technique is limited to small oxygen concentrations and requires a solid silicate phase.

In addition to the direct comparison at 134 GPa and 3200 K, we show our suite of calculations alongside previous results (Frost et al., 2010; Ozawa et al., 2008) for the partitioning of FeO between ferropericlase and liquid iron. Although they are at different conditions and therefore cannot be compared directly, it is clear that both sets of results broadly follow the same trend (Figure 1). The overall magnitude and spread of our $T = 3200$ K data are consistent with the available solid silicate-liquid metal partitioning experiments at similar temperature (Figure 1), demonstrating the general consistency between the two approaches.

Our results show that $K_D(O)$ increases strongly with temperature, as found previously (Fischer et al., 2015; Frost et al., 2010; Tsuno et al., 2013). In the absence of Si $K_D(O)$ is a weak function of $\bar{c}_O^c$ in the range $0 \leq \bar{c}_O^c \leq 30$ mol%, while adding 7.6% Si produces a strong increase of $K_D(O)$ with $\bar{c}_O^c$ (see also Table 1). This is consistent with extrapolations from previous work (Fischer et al., 2015; Tsuno et al., 2013), which predict high O and Si concentrations in the metal at high temperature.

4. Discussion

Transfer of O from mantle to core must be limited in some way or their bulk compositions would be in equilibrium by now (Stevenson, 1981): values of $\bar{c}_O^c$ between 2.5 and 28 mol% together with the calculated values of $K_D(O)$ require at most 2.5% FeO in coexisting (Mg,Fe)O (Table 1), which is less than one third of the expected FeO concentration in ferropericlase at lower mantle conditions (Asahara et al., 2007). This conclusion is consistent with previous work (Buffett & Seagle, 2010) using partitioning results extrapolated based on the thermodynamic model of Frost et al. (2010). One plausible resolution to this apparent paradox is that
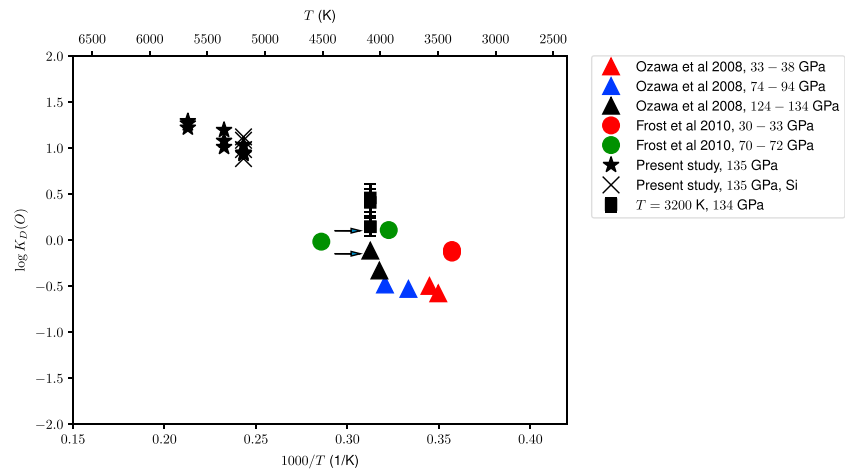
Figure 1. Comparison of our results with published work. Our data are plotted together with other experimental studies of solid silicate-liquid metal partitioning. The arrows highlight the direct comparison discussed in the text between a present calculation and a previous experimental determination of $K_D(O)$ at the same pressure-temperature conditions.

the top of the core is enriched in O compared to the bulk due to FeO transfer across the CMB (Frost et al., 2010) with the base of the mantle depleted in FeO compared to the bulk (Figure 2).

The crucial dynamical quantity is the mass flux of FeO. The chemical reaction is fast, and radial motion near the CMB must be significantly restricted, so the rate must be controlled kinetically by diffusion. Fick's law of mass diffusion relates the flux of FeO per unit area, i_{FeO}, to the mass fraction of Fe in ferropericlase, c_{Fe}^m, according to

$$i_{FeO} = -\rho^m D^m \nabla c_{Fe}^m, \tag{6}$$

where $\rho^m \approx 5500$ kg/m^3 is the lower mantle density (Dziewonski & Anderson, 1981) and $D^m = O(10^{-12} - 10^{-16})$ m^2/s is the diffusion constant of FeO in the solid mantle (Ammann et al., 2010). Recall that the mass
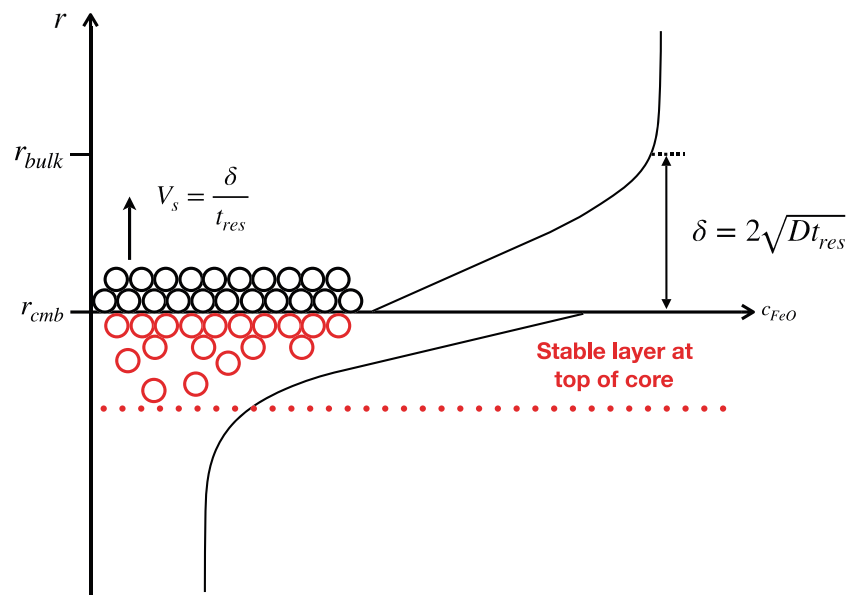

Figure 2. Illustration of chemical exchange between the lower mantle and core. FeO-rich material can be brought into contact with the core by diffusion or buoyancy. Diffusion depletes the lower mantle through a skin depth of thickness $\delta = 2\sqrt{Dt_{res}}$, where D is the diffusion coefficient and t_{res} the residence time for undepleted material at the core-mantle boundary (CMB). The top of the layer is at radius r_{bulk} and the base of the layer is the CMB radius r_{cmb}. Buoyant FeO-depleted material rises with the Stokes velocity V_s. Passage of FeO across the CMB creates a stably stratified layer (red) at the top of the core.

fraction of FeO in ferropericlase is determined by the mass fraction of Fe. We are interested in the flux of O, $i_O = i_{FeO}A_O/A_{FeO}$, where the factor $A_O/A_{FeO} = 16/72$ converts from FeO to O using the atomic weights of O (A_O) and FeO (A_{FeO}). The total mass flux of O across the CMB is $I_O = 4\pi r_{cmb}^2 i_O$, where r_{cmb} is the CMB radius, and so

$$I_O = -4\pi r_{cmb}^2 \rho^m D^m \nabla c_{Fe}^m \frac{A_O}{A_{FeO}}. \tag{7}$$

At the present day, I_O is limited by the minute chemical diffusivity (Ammann et al., 2010; Holzapfel et al., 2005) in the solid mantle. For a typical lower mantle flow speed of 1 cm/year diffusion will deplete mantle material through a skin depth $\delta = 2\sqrt{D^m t_{res}}$, where t_{res} is the residence time for undepleted material at the CMB (Figure 2). We therefore write $\nabla c_{Fe}^m \approx [c_{Fe}^m(r_{bulk}) - c_{Fe}^m(r_{cmb})]/\delta$, where r_{bulk} is the radius at the top of the lower mantle chemical boundary layer. The total mass flux of O into the core is then

$$I_O \approx 2\pi r_{cmb}^2 \rho^m \left[c_{Fe}^m(r_{cmb}) - c_{Fe}^m(r_{bulk}) \right] \sqrt{\frac{D^m}{t_{res}}} \frac{A_O}{A_{FeO}}. \tag{8}$$

For complete depletion of the layer in contact with the core, $c_{Fe}^m(r_{cmb}) = 0$. Taking $c_{Fe}^m(r_{bulk}) = 0.2$, a high estimate of the FeO content of ambient lower mantle, $D^m = 10^{-12}$ m²/s and a nominal residence time of $t_{res} = 10$ Myrs gives $\delta \approx 30$ m and an O flux of $\approx 1{,}000$ kg/s. This is smaller than the O flux down the core pressure gradient (Gubbins & Davies, 2013) and the result of Buffett and Seagle (2010), which was based on the thermodynamic model of Frost et al. (2010) calibrated at 25 GPa. It would be smaller still using the lower values of D^m and higher values of t_{res}.

Passage of FeO into the core by solid-state diffusion is therefore negligible, but mantle material depleted in FeO is buoyant and potentially able to rise, driving convection to aid removal of iron from the CMB (Figure 2). The rise time of a spherical parcel of depleted mantle, radius $\delta/2$, rising at the Stokes velocity $V_s = \rho^m \left[c_{Fe}^m(r_{cmb}) - c_{Fe}^m(r_{bulk}) \right] g\delta^2 A_O/18\mu A_{FeO}$, is δ/V_s. Removal is consistent when $\delta/V_S = t_{res}$. The mass flux decreases with increasing dynamic viscosity μ and decreasing D^m. For $\mu = 10^{19}$ Pa s, a rather low value, and other numbers as above we obtain $\delta = 66$ m, $t_{res} = 35$ Myrs and $V_s = 6\times 10^{-14}$ m/s. Compared to the previous estimates, the mass flux is increased by the larger δ but decreased by the longer t_{res}, the overall effect being a reduction by a factor of 2. The boundary layer remains intact until global mantle convection carries the material upward. Other processes such as erosion (Buffett et al., 2000) may expose fresh mantle to react with the core, or partial melt associated with ultralow velocity zones (Williams & Garnero, 1996) could aid migration, increasing the estimates above. However, both estimates suggest that the solid mantle limits the passage of oxygen into the core to small amounts.

Buffett and Seagle (2010) and Gubbins and Davies (2013) found that the flux of O creates a stabilizing compositional gradient at the top of the core that is too strong to allow material entrainment or mixing by the underlying convection. They both found stable layers approximately 100-km thick at the present day that formed over the age of the Earth, which are thinner than the estimates of 300–700 km from some seismic studies (Helffrich & Kaneshima, 2010; Kaneshima, 2017). The reduced O flux found here will further reduce the stable layer thickness below the seismic estimates.

FeO dissociation is accompanied by heat absorption at the CMB. The reaction is endothermic because the heat of reaction coefficient $R_h = \mu - T(\partial\mu/\partial T)_{P,T} > 0$, consistent with fitting to experimental data (Asahara et al., 2007). In our calculations this arises from the strong temperature dependence of the chemical potential difference (Table 1). The reaction does not directly power the geodynamo because it occurs at the CMB where heat is extracted; however, it provides power indirectly by augmenting the CMB heat flow. The additional power is proportional to i_O and is therefore small for transfer from a solid mantle.

The amount of oxygen delivered to the core could be altered by several factors, including the presence of other elements, a primordial chemical stratification established during core formation (Jacobson et al., 2017; Landeau et al., 2016) or the existence of an early partially molten layer at the base of the mantle (Brodholt & Badro, 2017; Labrosse et al., 2007). Extrapolations of experimental results to core conditions suggest that Ni and S have little effect (Tsuno et al., 2011). Si might also accompany O into the core in significant amounts (Tsuno et al., 2013), though future calculations will need to include bridgmanite to assess the role of Si at CMB conditions. Partitioning behavior at high concentrations must be calculated since our calculations do not rule out the possibility that O transfer could saturate or even reverse direction if the top of the core evolves to a pure FeO composition.

A stable chemical layer produced during core formation (Landeau et al., 2016) may reduce subsequent FeO exchange if it is enriched in oxygen. The composition of any such layer is currently uncertain, and therefore, this scenario cannot presently be investigated in detail. Another significant question is whether such a layer could survive the final stages of core formation, with recent work suggesting that it may have been erased by the moon-forming impact (Jacobson et al., 2017).

Core thermal history calculations with high thermal conductivity predict that the lowermost mantle would have been molten for a substantial fraction of Earth's history (Davies, 2015; Nimmo, 2015). In this scenario the oxygen flux through the molten lower mantle boundary layer would be greatly enhanced compared to the solid owing to the vastly reduced liquid viscosity and thermal diffusivity (Brodholt & Badro, 2017), though the oxygen partition coefficient would decrease since iron is more readily accommodated in a melt than a solid phase (Andrault et al., 2012; Nomura et al., 2011). The net effect depends on these two factors, though we expect the enhanced oxygen flux to win out. This scenario has the potential to transfer a significant amount of O into the core.

To estimate the mass flux from a molten lower mantle, we use equation (8) and assume a value of $D^m \sim 10^{-8}$–10^{-9} m^2/s obtained for diffusion of O in liquid iron (Gubbins et al., 2004; Posner et al., 2017). Convective velocities on the order of 1–10 m/s have been estimated for the magma ocean (Solomatov, 2015; Ziegler & Stegman, 2013), suggesting values of t_{res} in the range 10^{-2}–10^2 years. Since radial flow should be impeded in the vicinity of the CMB we assume the range $t_{\text{res}} = 100$–1,000 years, which gives $I_O \sim 10^5$–10^7, 2–4 orders of magnitude higher than for the solid. Lower values of t_{res} would increase this estimate further. In the stable region below the CMB the mass fraction of O, c_O^c, satisfies the diffusion equation,

$$\frac{\partial c_O^c}{\partial t} = D^c \nabla^c c_O^c, \tag{9}$$

where $D^c \sim 10^{-8}$–10^{-9} m^2/s is the O diffusion coefficient in the core (Davies et al., 2015; Gubbins et al., 2004). We use an analytical solution to this equation that applies in an infinite half-space with a time-independent flux at the CMB. The solution for the concentration gradient is standard and can be written (Gubbins & Davies, 2013, equation(12))

$$\frac{\partial c_O^c}{\partial r} = \frac{i_O}{(\rho^c D^c)} \text{erfc}([r_{\text{cmb}} - r]/2\sqrt{(D^c t)}), \tag{10}$$

where $\rho^c = 9,900$ kg/m^3 (Dziewonski & Anderson, 1981) is the density at the CMB. This solution is valid for thin layers of $O(100)$ km (Gubbins & Davies, 2013) as expected at the top of the core. The base of the stable layer is defined as the point where $\partial c_O^c / \partial r$ equals the destabilizing gradient, $\partial C/\partial r$, due to core convection. Following Buffett and Seagle (2010), we set $\partial C/\partial r = -\alpha_T/\alpha_c \partial T/\partial r$, where $\alpha_T = 2 \times 10^{-5}$ K^{-1} is the thermal expansion coefficient (Gubbins et al., 2003), $\alpha_c = 1.1$ is the expansion coefficient for O, and $\partial T/\partial r \sim 10^{-3} - 10^{-4}$ K/m is the superadiabatic temperature gradient (Davies et al., 2015; Nimmo, 2015).

As an example we assume that a molten lower mantle persisted for time $t = 1$ billion years following core formation. With the range of values above we find that the layer thickness at this time is between 75 and 125 km, significantly thicker than the 20–60 km obtained by the same calculation using the estimates of flux from a solid mantle above or the value of ~40 km obtained at this time by Buffett and Seagle (2010). The thickest layers may overestimate the effect since continual enrichment of the top of the core in O will reduce the concentration difference across the chemical boundary layer, reducing the mass flux. On the other hand, larger values of t_{res} would increase the layer thickness. Nevertheless, this simple calculation demonstrates the potential significance of a long-lived basal magma ocean (Labrosse et al., 2007) for core-mantle chemical exchange and paves the way for more sophisticated models that couple the time-dependent chemical boundary layers on both sides of the CMB.

References

Alfè, D. (2009). PHON: A program to calculate phonons using the small displacement method. *Computer Physics Communication*, *180*, 2622–2633.

Alfè, D., Gillan, M., & Price, G. (2002). Composition and temperature of the Earth's core constrained by combining ab initio calculations and seismic data. *Earth and Planetary Science Letters*, *195*, 91–98.

Ammann, M., Brodholt, J., Wookey, J., & Dobson, D. (2010). First-principles constraints on diffusion in lower-mantle minerals and a weak D''. *Nature*, *465*, 462–465.

Andrault, D., Petitgirard, S., Lo Nigro, G., Devidal, J.-L., Veronesi, G., Garbarino, G., & Mezouar, M. (2012). Solid-liquid iron partitioning in Earth's deep mantle. *Nature*, *487*(7407), 354–357. https://doi.org/10.1038/nature11294

Anzellini, S., Dewaele, A., Mezouar, M., Loubeyre, P., & Morard, G. (2013). Melting of iron at Earth's inner core boundary based on fast X-ray diffraction. *Science*, *340*, 464–466.

Asahara, Y., Frost, D. J., & Rubie, D. C. (2007). Partitioning of FeO between magnesiowustite and liquid iron at high pressures and temperatures: Implications for the composition of the Earth's outer core. *Earth and Planetary Science Letters*, *257*, 435–449.

Badro, J., Brodholt, J., Piet, H., Siebert, J., & Ryerson, F. (2015). Core formation and core composition from coupled geochemical and geophysical constraints. *Proceedings of the National Academy of Sciences*, *112*, 12,310–12,314.

Badro, J., Côté, A., & Brodholt, J. (2014). A seismologically consistent compositional model of Earth's core. *Proceedings of the National Academy of Sciences*, *111*, 7542–7545.

Brodholt, J., & Badro, J. (2017). Composition of the low seismic velocity E' layer t the top of Earth's core. *Geophysical Research Letters*, *44*, 8303–8310. https://doi.org/10.1002/2017GL074261

Buffett, B., Garnero, E., & Jeanloz, R. (2000). Sediments at the top of Earth's core. *Science*, *290*, 1338–1342.

Buffett, B., & Seagle, C. (2010). Stratification of the top of the core due to chemical interactions with the mantle. *Journal of Geophysical Research*, *115*, B04407. https://doi.org/10.1029/2009JB006751

Davies, C. (2015). Cooling history of Earth's core with high thermal conductivity. *Physics of the Earth and Planetary Interiors*, *247*, 67–79.

Davies, C., Pozzo, M., Gubbins, D., & Alfè, D. (2015). Constraints from material properties on the dynamics and evolution of Earth's core. *Nature Geoscience*, *8*, 678–687.

Dziewonski, A., & Anderson, D. (1981). Preliminary reference Earth model. *Physics of the Earth and Planetary Interiors*, *25*, 297–356.

Fischer, R. A., Nakajima, Y., Campbell, A. J., Frost, D. J., Harries, D., Langenhorst, F., et al. (2015). High pressure metal-silicate partitioning of Ni, Co, V, Cr, Si, and O. *Geochimica et Cosmochimica Acta*, *167*(Supplement C), 177–194.

Frost, D., Asahara, Y., Rubie, D. C., Miyajima, N., Dubrovinsky, L. S., Holzapfel, C., et al. (2010). Partitioning of oxygen between the Earth's mantle and core. *Journal of Geophysical Research*, *115*, B02202. https://doi.org/10.1029/2009JB006302

Garnero, E., McNamara, A., & Shim, S.-H. (2016). Continent-sized anomalous zones with low seismic velocity at the base of Earth's mantle. *Nature Geoscience*, *9*, 481–489.

Geßmann, C., & Rubie, D. C. (1998). The effect of temperature on the partitioning of nickel, cobalt, manganese, chromium, and vanadium at 9 GPa and constraints on formation of the Earth's core. *Geochimica et Cosmochimica Acta*, *62*(5), 867–882.

Gubbins, D., Alfe, D., Masters, G., Price, G., & Gillan, M. (2003). Can the Earth's dynamo run on heat alone? *Geophysical Journal International*, *155*, 609–622.

Gubbins, D., Alfè, D., Masters, G., Price, G., & Gillan, M. (2004). Gross thermodynamics of two-component core convection. *Geophysical Journal International*, *157*, 1407–1414.

Gubbins, D., & Davies, C. (2013). The stratified layer at the core-mantle boundary caused by barodiffusion of oxygen, sulphur and silicon. *Physics of the Earth and Planetary Interiors*, *215*, 21–28.

Helffrich, G., & Kaneshima, S. (2010). Outer-core compositional stratification from observed core wave speed profiles. *Nature*, *468*, 807–809. https://doi.org/10.1038/nature09636

Hirose, K., Labrosse, S., & Hernlund, J. (2013). Compositional state of Earth's core. *Annual Review of Earth and Planetary Sciences*, *41*, 657–691.

Holzapfel, C., Rubie, D. C., Frost, D., & Langenhorst, F. (2005). Fe-Mg interdiffusion in (Mg, Fe) SiO$_3$ perovskite and lower mantle reequilibration. *Science*, *309*(5741), 1707–1710.

Jacobson, S. A., Rubie, D. C., Herlund, J., Morbidelli, A., & Nakajima, M. (2017). Formation, stratification, and mixing of the cores of Earth and Venus. *Earth and Planetary Science Letters*, *474*, 375–386.

Kaneshima, S. (2017). Array analysis of SmKS waves and stratification of Earth's outermost core. *Physics of the Earth and Planetary Interiors*, *223*, 2–7.

Knittle, E., & Jeanloz, R. (1991). Earth's core-mantle boundary: Results of experiments at high pressures and temperatures. *Science*, *251*, 1438–1443.

Labrosse, S., Hernlund, J., & Coltice, N. (2007). A crystallizing dense magma ocean at the base of the Earth's mantle. *Nature*, *450*, 866–869.

Landeau, M., Olson, P., Deguen, R., & Hirsh, B. H. (2016). Core merging and stratification following giant impact. *Nature Geoscience*, *9*, 786–789. https://doi.org/10.1038/NGEO2808

Masters, G., & Gubbins, D. (2003). On the resolution of density within the Earth. *Physics of the Earth and Planetary Interiors*, *140*, 159–167.

Nimmo, F. (2015). Energetics of the core. In G. Schubert (Ed.), *Treatise on geophysics 2nd edn* (Vol. 8, pp. 27–55). Amsterdam: Elsevier.

Nomura, R., Ozawa, H., Tateno, S., Hirose, K., Hernlund, J., Muto, S., et al. (2011). Spin crossover and iron-rich silicate melt in the Earth's deep mantle. *Nature*, *473*(7346), 199–202. https://doi.org/10.1038/nature09940

O'Neill, H., Canil, D., & Rubie, D. C. (1998). Oxide-metal equilibria to 2500° C and 25 GPa: Implications for core formation and the light component in the Earth's core. *Journal of Geophysical Research*, *103*(B6), 12,239–12,260.

Ozawa, H., Hirose, K., Mitome, M., Bando, Y., Sata, N., & Ohishi, Y. (2008). Chemical equilibrium between ferropericlase and molten iron to 134 GPa and implications for iron content at the bottom of the mantle. *Geophysical Research Letters*, *35*, L05308. https://doi.org/10.1029/2007GL032648

Posner, E., Rubie, D. C., Frost, D. J., & Steinle-Neumann, G. (2017). Experimental determination of oxygen diffusion in liquid iron at high pressure. *Earth and Planetary Science Letters*, *464*, 116–123.

Rubie, D. C., Jacobson, S. A., Morbidelli, A., O'Brien, D. P., Young, E. D., de Vries, J., et al. (2015). Accretion and differentiation of the terrestrial planets with implications for the compositions of early-formed Solar System bodies and accretion of water. *Icarus*, *248*, 89–108. https://doi.org/10.1016/j.icarus.2014.10.015

Rubie, D. C., Nimmo, F., & Melosh, H. J. (2015). Formation of Earth's Core. In G. Schubert (Ed.), *Treatise on geophysics 2nd edn* (Vol. 9, pp. 43–79). Amsterdam: Elsevier.

Solomatov, V. (2015). Magma oceans and primordial mantle differentiation. In G. Schubert (Ed.), *Treatise on geophysics 2nd edn* (Vol. 10, pp. 81–104). Amsterdam: Elsevier.

Stevenson, D. J. (1981). Models of the Earth's core. *Science*, *214*(4521), 611–619.

Takafuji, N., Hirose, K., Mitome, M., & Bando, Y. (2005). Solubilities of O and Si in liquid iron in equilibrium with (Mg, Fe)SiO$_3$ perovskite and the light elements in the core. *Geophysical Research Letters*, *32*, L06313. https://doi.org/10.1029/2005GL022773

Tsuno, K., Frost, D. J., & Rubie, D. C. (2011). The effects of nickel and sulphur on the core–mantle partitioning of oxygen in Earth and Mars. *Physics of the Earth and Planetary Interiors*, *185*, 1–12.

Tsuno, K., Frost, D. J., & Rubie, D. C. (2013). Simultaneous partitioning of silicon and oxygen into the Earth's core during early Earth differentiation. *Geophysical Research Letters*, *40*, 66–71. https://doi.org/10.1029/2012GL054116

Williams, Q., & Garnero, E. J. (1996). Seismic evidence for partial melt at the base of Earth's mantle. *Science*, *273*(5281), 1528–1530.

Ziegler, L. B., & Stegman, D. R. (2013). Implications of a long-lived basal magma ocean in generating Earth's ancient magnetic field. *Geochemistry, Geophysics, Geosystems*, *14*, 4735–4742. https://doi.org/10.1002/2013GC005001